Red Blood Cell (RBC) aggregation and its influence on non-Newtonian nature of blood in microvasculature.

Chitra Murali and Perumal Nithiarasu*
Computational Biomedical Engineering and Rheology Group
Zienkiewicz Centre for Computational Engineering
College of Engineering, Swansea University, Swansea, UK

November 9, 2016

Abstract

A robust computational model is proposed to investigate the non-Newtonian nature of blood due to rouleaux formation in microvasculature. The model consists of appropriate forces responsible for red blood cell (RBC) aggregation in the microvasculature, tracking of RBCs, and coupling between plasma flow and RBCs. The RBC aggregation results have been compared against the available data. The importance of different hydrodynamic forces on red blood cell aggregation has been delineated by comparing the time dependent path of the RBCs. The rheological changes to the blood have been investigated under different shear rates and hematocrit values and quantified with and without RBC aggregation. The results obtained in terms of wall shear stress (WSS) and blood viscosity indicate a significant difference between Newtonian and powerlaw fluid assumptions.

Keywords: Red blood cell , rouleaux ,microcirculation , wall shear stress , blood flow, non-newtonian

1 Introduction

The red blood cell (RBC) is an important constituent of blood and it is often responsible for making the flow non-Newtonian in small vessels. Its aggregation has substantial influence on *in vivo* haemodynamics and can adversely affect the red blood cell distribution and flow dynamics in the microcirculation[1, 2, 3]. In addition to filling capillaries and making these capillaries dysfunctional over time[1], the RBC aggregation has also been found to change the blood viscosity and decrease the density of functional capillaries[3]. It is clear from viscometric measurements that the apparent blood viscosity rises with decreasing shear rates[4, 5]. It has also been shown that RBC aggregation plays a vital role in determining the blood viscosity at low shear rates [5]. This is due to the fact that RBC aggregation is a major determinant of the shear thinning property of the blood. In addition, axial migration of RBC aggregates along with plasma skimming represents a phase separation and formation of a marginal cell-poor fluid zone near the vessel walls [6]. This phenomenon leads to an alteration of the average hematocrit value of the blood in the branching vessels [7]. Hence the average hematocrit of the blood in small vessels is lower than the hematocrit value measured in the blood obtained from a large vein or artery[8].

In addition to the mentioned impact of RBC aggregation on vasculature, it is one of the important factors responsible for low shear stress regions. It is apparent that persistent exposure to low shear stress, as a consequence of poor blood circulation, leads to cardiovascular diseases[9]. It is also known that low wall shear stress (WSS) regions are often responsible for lesion formation, occlusion and thrombosis, both in arterial and venuous systems[10]. In addition, enhanced RBC aggregation and low WSS leads to reduction in NO synthesis and also causes disturbed vascular tone[11]. While RBC aggregation or rouleaux is directly or

*Author for correspondence, e-mail: P.Nithiarasu@swansea.ac.uk

indirectly responsible for some cardiovascular diseases, its formation may be influenced by hereditary blood disorders, as well as diseases such as diabetes, sickle cell anemia and malaria[12]. All these diseases result in reduced RBC deformability with increased viscosity and the onset and progression of the pathological state. Other diseases that influence RBC aggregation include sepsis, myocardial ischaemia and renal failure[13].

As seen, understanding RBC aggregation is undoubtedly one of the important and useful topics within microcirculation. However, *in vivo* measurements of RBC aggregation are extremely difficult to carryout. Thus, computational models assume prominence in developing a better understanding. Although some data is now available on the physiological and clinical importance of RBC aggregation phenomenon, its formation and transport still is one of the poorly understood areas.

In general two approaches are adapted for modelling the red blood cells. The first is an implicit approach in which the red blood cells are treated as points with imaginary membranes, and the second is an explicit approach in which the RBC is described using full membrane models. The latter is a detailed approach that is required for investigating small groups of RBCs. For large number of RBCs, this approach is very expensive and obtaining a sensible result within a reasonable amount of time is difficult [14, 15, 16, 17, 18]. Thus, an implicit approach that models RBCs as points is often preferred for aggregation studies.

The implicit models treat the RBCs as elliptical particles and the blood cell aggregations in general is based upon a force balance between fluid forces and the natural adhesion forces between them. The adhesion forces between RBCs is the result of receptor-ligand bonding between the cells [19, 20, 21, 22]. Such a model is built based on a combination of experimental data and computational techniques. The fluid forces used normally consists of the drag resistance induced by the flow [21, 22]. In an uniform and irrotational flow, drag resistance alone is valid and accurate. However, when blood flow is disturbed (for example in the vicinity of bifurcations and stenoses), the lift forces may also play as significant role as drag forces. In addition, the difference in timescales between flow and physical process of aggregation is large. Hence, multi-time step procedure is essential to capture the rouleaux formation [23].

It is clear from the studies based on *in vitro* [24] and *in vivo* experiments that aggregation has a significant influence on the velocity profiles in microvessels [25, 2, 26]. However, such change in velocity profile may not be easily implemented in an implicit model as the coupling between flow and aggregation is one directional. One of the best options to induce such a velocity profile change is through the introduction of non-Newtonian nature, enacted by RBC aggregation. As mentioned earlier, rheological characteristics of blood flow in arteries are influenced by the strength of aggregation. Hence, it is important to incorporate the effect of local RBC concentration while solving the flow model. We propose that shear thinning behaviour of blood flow and haemorheological changes, in the presence of RBC aggregations, may be quantified using a power law model. Although the hematocrit values have been incorporated into the computational model in the past to evaluate the shear dependent viscosity in the venular bifurcation [27, 28], such studies failed to integrate particle dynamics and RBC aggregation structure. Such models are useful tools for simple situations but may not be very relevant for physiological situations without the inclusion of an aggregation model.

The objective of the present work is therefore two fold. The first objective is to improve the existing models for predicting RBC aggregation using a comprehensive framework that uses both drag and lift forces of the particles and different time scales. Such a comprehensive model is then applied to predict the non-Newtonian nature of the blood flow using a powerlaw model as the basis, which is valid for low Reynolds number flows [29, 30].

2 Methodology

In the present model, dynamics of the blood plasma is obtained by solving the incompressible Navier-stokes equations and assuming that the flow is Newtonian[31, 32, 30]. The RBC's in the blood, represented using elliptical shapes, are suspended in the plasma in a two-dimensional computational domain. These RBCs are allowed to move with the plasma and interact. The movement of these particles is tracked using RBC dynamics and forces responsible for aggregation. A collision detection method along with a differential time stepping method to determine adhesion forces is used in modelling RBC aggregation. The influence of RBC aggregation on the surrounding flow field, is introduced into the flow model through an aggregation

parameter. To determine the influence of RBC aggregation on the flow nature, a powerlaw model has been incorporated into the flow model for the computation of shear dependent viscosity, which is suitable for low shear flows [29, 30]. The following subsections provide a brief description of various components of the model employed.

2.1 Fluid dynamics

The Characteristics Based Split (CBS) scheme has been adopted [31] for solving the incompressible Navier-Stokes equations using the finite element method. This consists essentially of three steps. In the first step, an intermediate velocity field is established without considering the pressure. The pressure is obtained in the second step by solving a modified continuity equation and finally the intermediate velocities are corrected to obtain the final velocities. Further details on the CBS method and higher order dual time stepping can be found in [32] and [31]. For transient flows, the dual time stepping gives at least second order accuracy for all variables.

2.2 Particle kinematics in two dimension

Studying the flow induced motion of the RBCs, suspended in the moving flow field, requires a convenient representation. This requires three different coordinate systems to work in concert to produce a desired result. They are the Cartesian coordinates of the Eulerian flow field, $\mathbf{X} = [x, y]$, which are non-rotating, inertial coordinates. The local particle coordinates are given as $\hat{\mathbf{X}} = [\hat{x}, \hat{y}]$, with the origin placed at the particle centre. This coordinate is used to describe the rotation of the particle and it coincides with the principal axes of the particle every time step. The third coordinate system required is $\hat{\hat{\mathbf{X}}} = [\hat{\hat{x}}, \hat{\hat{y}}]$ with its origin coinciding with that of the particle frame and its axes parallel to the corresponding inertial frame (Figure 1). This third coordinate system is referred to as the co-moving frame. The transformation between the co-moving frame coordinates and particle frame coordinates is given as a linear relation [33] , i.e.,

$$\hat{\mathbf{X}} = \mathbf{A}\hat{\hat{\mathbf{X}}} \tag{1}$$

The transformation matrix, $\mathbf{A}$, may be expressed using Euler angles and Euler four parameters, i.e,

$$\mathbf{A} = \begin{bmatrix} 1 - 2(\xi_2^2 + \xi_3^2) & 2(\xi_1\xi_2 + \xi_3\eta) \\ 2(\xi_2\xi_1 - \xi_3\eta) & 1 - 2(\xi_3^2 + \xi_1^2) \end{bmatrix} \tag{2}$$

here, $\xi_1, \xi_2, \xi_3, \eta$ are Euler's four parameters calculated from inital orientations using Euler angles in the co-moving frame as $\xi_1 = cos\frac{\varphi-\psi}{2}sin\frac{\theta}{2}$, $\xi_2 = sin\frac{\varphi-\psi}{2}sin\frac{\theta}{2}$, $\xi_3 = sin\frac{\varphi+\psi}{2}cos\frac{\theta}{2}$ and $\xi_3 = cos\frac{\varphi+\psi}{2}cos\frac{\theta}{2}$ and at subsequent time steps these are evolved as,

$$\begin{bmatrix} d\xi_1/dt \\ d\xi_2/dt \\ d\xi_3/dt \\ d\eta/dt \end{bmatrix} = \frac{1}{2}\begin{bmatrix} \xi_2\Omega_{\hat{z}} \\ -\xi_1\Omega_{\hat{z}} \\ \eta\Omega_{\hat{z}} \\ -\xi_3\Omega_{\hat{z}} \end{bmatrix} \tag{3}$$

where, $\Omega_{\hat{z}}$ is the RBC angular velocity or rotation in the particle frame, calculated in the following section. The transformation matrix $\mathbf{A}$ in Equation 2 is used in representing the forces in the appropriate coordinates as explained later.

2.3 Particle dynamics

Equation of motion of particles are described as linear and angular momentum of the particle mass centre, i.e.,

Momentum equation

$$m\frac{D\mathbf{v}}{Dt} = \mathbf{F}_F + \mathbf{F}_A \tag{4}$$

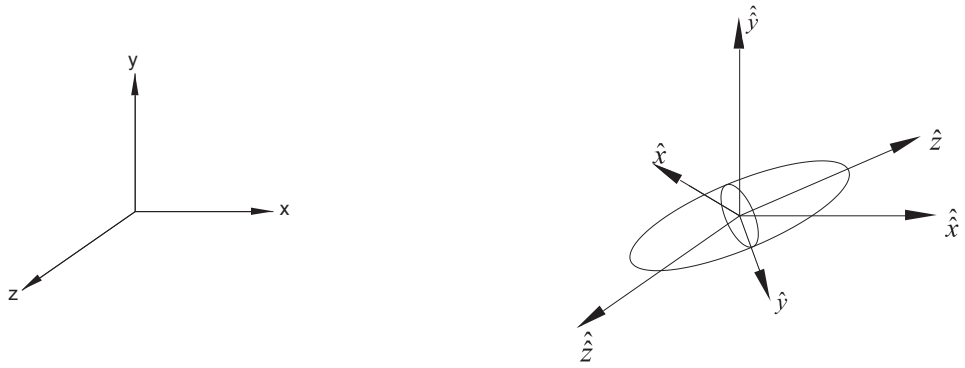

(a)

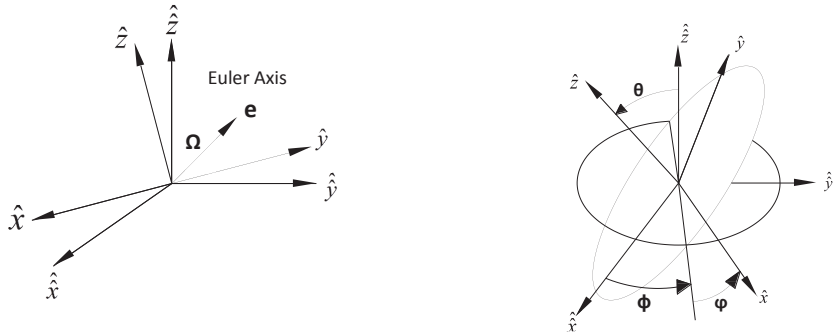

(b)

Figure 1: (a) An ellipsoidal particle with inertial coordinate system, (b) Euler angles and Euler parameters (particle frame and co-moving frame)

where, m is mass of an RBC, $\mathbf{v}$ velocity vector $\mathbf{F}_F$ the fluid and $\mathbf{F}_A$ the adhesion forces respectively.

Angular Momentum

$$I_{\hat{z}} \frac{D\Omega_{\hat{z}}}{Dt} = M_{F,\hat{z}} + M_{A,\hat{z}} \tag{5}$$

In the above equation, $I_{\hat{z}} = \frac{1}{5}m(a^2 + b^2)$ is the moment of inertia of RBCs, $\Omega_{\hat{z}}$ the rotation, $M_{F,\hat{z}}$ and $M_{A,\hat{z}}$ are moments due to fluid and adhesion forces respectively.

2.4 Hydrodynamic forces

Hydrodynamic forces include drag and lift forces on the RBCs. They are given as:

(i) Drag force

In a general flow field, the hydrodynamic drag force acting on an ellipsoidal particle is obtained in the form of an infinite series of fluid velocity and its spatial derivatives[34]. The higher order terms are proportional to higher order powers of particle minor axis. The first term of the series for small particles is,

$$\mathbf{F}_d = \mu b \pi \hat{\hat{\mathbf{K}}} (\mathbf{u} - \mathbf{v}) f \tag{6}$$

where, $\mathbf{u}$ is the fluid velocity vector at the RBC centroid, $\mathbf{v}$ is the RBC velocity vector, and $f = (1 - C(x,t))^{-3.7}$ is the particle crowding factor with $C(x,t)$ being particle volumetric concentration[35] (defined in Section 3.1) and b the particle semi-minor axis. In the equation 6, $\hat{\hat{\mathbf{K}}}$ is translation dyadic or resistance tensor given as,

$$\hat{\hat{\mathbf{K}}} = \mathbf{A}^{-1} \hat{\mathbf{K}} \mathbf{A} \tag{7}$$

The particle frame translation dyadic $\hat{\mathbf{K}} = [\hat{k}_{ij}]$ for an ellipse revolving about the $\hat{z}$ axis is a diagonal matrix [36] given as,

$$\hat{k}_{xx} = \hat{k}_{yy} = \frac{16(\beta^2 - 1)}{[(2\beta^2 - 3) ln(\beta + \sqrt(\beta^2 - 1))/(\sqrt(\beta^2 - 1))] + \beta} \tag{8}$$

where $\beta = b/a$ is the RBC aspect ratio and a is the semi-major axis.

(ii) Shear induced lift force

The shear induced lift force on an arbitrary shaped particle in a channel has been adopted from [37] as,

$$\mathbf{F}_l = \frac{\pi^2 \mu a^2}{(\mu/\rho)^{1/2}} \frac{\frac{\partial u_x}{\partial y}}{\left|\frac{\partial u_x}{\partial y}\right|^{1/2}} \hat{\mathbf{K}} \mathbf{L} \hat{\mathbf{K}} \left(\mathbf{u}^L - \mathbf{v}\right) \tag{9}$$

where $\mathbf{u}^L = [u_x, 0, 0]$ is the reference flow for the lift and $\mathbf{L}$ is lift tensor adopted from[36].

$$\mathbf{L} = \begin{bmatrix} 0.0501 & 0.0329 \\ 0.0182 & 0.0173 \end{bmatrix} \tag{10}$$

The drag and lift forces together form the total fluid force $\mathbf{F_F}$ introduced in the Equation 4.

(iii) Torque

In addition to the drag and lift forces, flow induced torque on small particles, in the particle frame for a two dimensional flow is,

$$M_{F,\hat{z}} = \frac{16\pi\mu ab^2}{3\left(a^2\alpha_0 + b^2\beta_0\right)}\left[\left(a^2 - b^2\right)d_{\hat{y}\hat{x}} + \left(a^2 + b^2\right)\left(\omega_{\hat{y}\hat{x}} - \Omega_{\hat{z}}\right)\right] \tag{11}$$

where $M_{F,\hat{z}}$ is the fluid induced torque about the z axis in the third direction (Equation 5), a and b are semi-major and minor axes of an ellipse. In the particle frame, $d_{\hat{y}\hat{x}}$ and $\omega_{\hat{y}\hat{x}}$ are the component of rate deformation tensor and vorticity tensor respectively, given in indicial notation as

$$d_{ij} = \frac{1}{2}\left(\frac{\partial u_i}{\partial x_j} + \frac{\partial u_j}{\partial x_i}\right); \quad \text{and} \quad \omega_{ij} = \frac{1}{2}\left(\frac{\partial u_i}{\partial x_j} - \frac{\partial u_j}{\partial x_i}\right) \tag{12}$$

where u_i are the fluid velocity components.

2.5 Adhesive forces

RBC adhesion forces are computed often using the receptor-ligand binding model which is similar to the one developed by Bell [19]. The adhesion forces are mathematically analogues to van der Waals forces of attraction under certain simplifications. Receptor-Ligand binding with time dependent surface energy density [21], which is similar to the one reported by Bell [19] may be adapted for computing the surface energy density of the RBCs. The time dependent surface energy density is given as,

$$\gamma(t) = \frac{\sigma(X_b - l)^2}{2}\left[\int_0^1 N_b(t - t_0(s))sds\right]. \tag{13}$$

and Adhesion Force is,

$$\mathbf{F}_A = \sigma(X_b - l)\left[\int_0^1 N_b(t - t_0(s))sds\right]\mathbf{n}. \tag{14}$$

where, σ is a spring constant given in N/m, X_b is the gap thickness between the cell surfaces within the contact region, l is equilibrium gap thickness at which bond force vanishes, N_b is bond number density defined as the number of bonds per unit area of the contact region as a function of time, and s is circumference length of an elliptical particle. The number density is given as

$$N_b(t) = \frac{2Atanh\left[\frac{1}{2}(B^2 - 4AC)^{1/2}(t - t_0)\right]}{-Btanh\left[\frac{1}{2}(B^2 - 4AC)^{1/2}(t - t_0)\right] + ((B^2 - 4AC)^{1/2})} \tag{15}$$

where $A = k_f N_{l0} N_{r0}$, $B = -[k_f(N_{l0} + N_{r0}) + k_r]$, $C = k_f$, k_f and k_r are respectively the forward and reverse reaction rate coefficients, N_{l0} and N_{r0} are respectively the initial receptor and ligand densities on the membrane.

An alternative and equivalent form of the adhesion force, which is used in the present study, was provided by [21] and is given as

$$\mathbf{F}_A = F_n\mathbf{n} + F_s\mathbf{t_s} \tag{16}$$

where the normal force F_n is resulting from a combination of elastic repulsion of particles, viscous dissipation and adhesive binding. The tangential force F_s is the result of sliding action of RBCs in contact. The unit normal $\mathbf{n}$ and unit tangent $\mathbf{t_s}$ at the contact points are appropriately used to compute the adhesion force components in x and y direction. The JKR equations for normal elastic force between two colliding particles were recast by [38], in terms of contact region radius as

$$\frac{F_n}{F_c} = 4\left(\frac{\bar{a}}{\bar{a_0}}\right)^3 - 4\left(\frac{\bar{a}}{\bar{a_0}}\right)^{3/2} \tag{17}$$

here, F_c is the critical force required to separate two attached RBCs with corresponding critical overlap, δ_c, $\bar{a}$ is the contact region radius and $\bar{a_0} = \left(\frac{9\pi\gamma R^2}{E}\right)^{1/3}$ with R being the effective particle radius, i.e., $1/R = K^i + K^j$ with K^i and K^j being the respective positive mean curvatures of two RBCs i and j at contact points and E being the Young's Modulus of an RBC ($3.1 \times 10^7 dyne/cm^2$) [39]. The equations for the critical force and critical overlap are given respectively as[38]

$$F_c = 3\pi\gamma R \quad \text{and} \quad \delta_c = \frac{\bar{a_0}^2}{2\,(6)^{1/3}\,R} \tag{18}$$

where γ is the equilibrium surface energy density given by Equation 13. The ratio between normal and critical overlaps of RBCs is given as

$$\frac{\delta_n}{\delta_c} = 6^{1/3}\left[2\left(\frac{\bar{a}}{\bar{a_0}}\right)^2 - \frac{4}{3}\left(\frac{\bar{a}}{\bar{a_0}}\right)^{1/2}\right] \tag{19}$$

here δ_n is the normal overlap between the contact points of colliding particles and is positive for intersecting particles and negative for necking particles. Once collision between RBCs is detected (see Section 4 for collision detection), the ratios in equations 17 and 19 are computed. If these ratios are greater than unity, the particles are attached and if less than unity then they are detached. The remaining component needed to calculate the adhesion force in Equation 16 is F_s, given as

$$F_s = -k_T \int_{t_0}^{t} \mathbf{v}_s(\tau) d\tau.\mathbf{t_s} - \eta_T \mathbf{v}_s.\mathbf{t_s} \tag{20}$$

where $k_T = 8G\bar{a}$ is the tangential stiffness coefficient [40] with G being the shear modulus of an RBC, $\mathbf{v}_s = \mathbf{v}_R - (\mathbf{v}_R.\mathbf{n})\mathbf{n}$ is the slip velocity, which is the tangent projection of $\mathbf{v}_R$ to the surface at the contact point,$\mathbf{t}_s = \mathbf{v}_s/\left|\mathbf{v}_s\right|$ is the slip direction, $\mathbf{v}_R = \mathbf{v}^i - \mathbf{v}^j + (\Omega^i \times r^i - \Omega^j \times r^j)$is the relative velocity of the particles at contact point and η_T is the viscous damping coefficient [41].

The last term required to compute the rotation of an RBC in Equation 5 is obtained from

$$\mathbf{M}_A = F_n(\mathbf{r}^i \times \mathbf{n}) + F_s r^i(\mathbf{n} \times \mathbf{t}_s) + M_r(\mathbf{t_R} \times \mathbf{n}) + M_t\mathbf{n} \tag{21}$$

The normal force produces a normal torque equal to $F_n\mathbf{r}^i \times \mathbf{n}$ and a sliding torque $F_s\mathbf{r}^i \times \mathbf{t}_s$. An associated torque acting on the particles due to resistance from twisting is $M_t\mathbf{n}$. In the presence of adhesion, particles experience strong resistance due to rolling as well. M_t is twisting resistance due to different rotation rate of two colliding particles in the direction $\mathbf{n}$. The relative twisting rate is defined as $\Omega_T = (\mathbf{\Omega}^i - \mathbf{\Omega}^j).\mathbf{n}$, $M_t = -k_T\bar{a}^2/2\int_{t_0}^{t}\Omega_T(\tau)d\tau - \eta_T\bar{a}^2/2\Omega_T$, M_r- rolling resistance induced asymmetry in the contact region, $M_r = -4F_c\bar{a}/\bar{a_0}^{(3/2)}\xi$-[42], $\xi = \int_{t_0}^{t}\mathbf{v}_L(\tau)d\tau.\mathbf{t}_R$ is the displacement of the particle centroid due to rolling in the $\mathbf{t}_R$ rolling direction, $\mathbf{t}_R = \mathbf{v}_L/\left|\mathbf{v}_L\right|$, $\mathbf{v}_L = (K^i + K^j)^{-1}\left\{(\mathbf{\Omega}^j - \mathbf{\Omega}^i) \times \mathbf{n} - (1/2)(K^i - K^j)\left[\mathbf{v}_R - (\mathbf{v}_R.\mathbf{n})\mathbf{n}\right]\right\}$ is the rolling displacement [43].

In summary, F_n is positive when two particles pushes towards each other and negative when move away from each other due to fluid force. Even for the negative values of δ_n the contact will be maintained untill the critical point is reached at which $F_n = -F_c$ and $\delta_n = -\delta_c$. For saving computational time F_n/F_c and $\bar{a}/\bar{a_0}$ can be precomputed as functions of δ_n/δ_c to determine F_n and $\bar{a}$ for given value of δ_n at each time step. In the equation 5 only the $'z'$ component of M_A is added.

3 Non-dimensional form of the equations

The non-dimensional form of the main equations may be obtained by employing following non-dimensional scales.

$$\mathbf{u}^* = \frac{\mathbf{u}}{U_\infty}, \mathbf{v}^* = \frac{\mathbf{v}}{U_\infty}, t^* = \frac{tU_\infty}{L}, \rho^* = \frac{\rho_p}{\rho_f}, l^* = \frac{l}{L},$$
$$R_e = \frac{\rho_f U_\infty L}{\mu_f}, \hat{\mathbf{K}}^* = \frac{\hat{\mathbf{K}}}{L}, \sigma^* = \frac{\sigma}{\rho_f {U_\infty}^2 L} \tag{22}$$

where, U_∞ is the reference velocity, L is a characteristic length, ρ_f is density of fluid (plasma), ρ_p is density of RBC and μ_f is dynamics viscosity of the fluid. Applying these scales give the following equations of motion of RBCs

$$\frac{d\mathbf{v}^*}{dt^*} = \frac{1}{\rho^* (l^*)^2} \left[\frac{k^*}{R_e} (\mathbf{u}^* - \mathbf{v}^*) + \frac{\pi^2 (\partial u_x^*/\partial y^*)(\mathbf{u}^* - \mathbf{v}^*)}{\rho^* Re^{(1/2)} |(\partial u_x^*/\partial y^*)|^{(1/2)}} + \sigma^* c_1 \right] \tag{23}$$

$$\frac{d{\Omega_{\hat{z}}}^*}{dt^*} = \frac{1}{m^*} (M_{F,\hat{z}}{}^* + M_{A,\hat{z}}{}^*) \tag{24}$$

$$M_{F,\hat{z}}{}^* = \frac{16\pi a^* {b^*}^2}{3({a^*}^2 \alpha_0 + {b^*}^2 \beta_0) Re} (({a^*}^2 - {b^*}^2) {d_{yx}}^* + ({a^*}^2 + {b^*}^2)({\omega_{yz}}^* - {\Omega_z}^*)) \tag{25}$$

$$M_A^* = {\mathbf{F_n}}^* {r_i}^* \times n + {\mathbf{F_s}}^* {r_i}^* \times \mathbf{t_s} + {M_t}^* n + {M_r}^* \mathbf{t_R} \times \mathbf{n} \tag{26}$$

M_A is given in the vector form to avoid the confusion. where, $c_1 = \int_0^1 N_b (t - t_0(s)) \, sds$, is Bond number density, s-circumference length of particle. In solving the equation of motion of particles involves three important steps, such as to find out Adhesion, Hydrodynamic forces (Drag and Lift force) and detect collision among the particles.

3.1 The modified Navier-Stokes equations and power law

The non-dimensional Navier-Stokes equations in the presence of RBCs may be written as (without asterisks) based on [44],

$$\frac{\partial (C_v \rho_f)}{\partial t} + \nabla . (C_v \rho_f u_i) = 0 \tag{27}$$

$$\frac{\partial (C_v \rho_f u_i)}{\partial t} + \frac{\partial (C_v \rho_f u_i u_j)}{\partial x_j} = -C_v \frac{\partial p}{\partial x_i} + \frac{1}{Re} \frac{\partial}{\partial x_j} \left[C_v \mu \left(\frac{\partial u_i}{\partial x_j} + \frac{\partial u_j}{\partial x_i} \right) \right] \tag{28}$$

Where $C_v = 1 - C(\mathbf{x}, t)$ is the voidage fraction, where particle concentration field $C(\mathbf{x}, t)$ is obtained by computing the particle concentration based on variant of particle cloud approach [23]. The contribution of the continuous particle concentration field from each particle can be distributed as a cloud around the particle centre as determined by a weighting function $f(\mathbf{x} - \mathbf{x_n}, R_n)$ such that the integral of f over all space equals to unity and R_n is a particle cloud radius assumed to be constant. The Gaussian function for f may be expressed as,

$$f(\mathbf{x} - \mathbf{x_n}, R_n) = \frac{2}{3\pi R_n^3} exp \left[- |\mathbf{x} - \mathbf{x_n}|^2 / R_n^2 \right] \tag{29}$$

The particle concentration $C(\mathbf{x}, t)$ at a point (x, y) is obtained by summing over contributions of all the particles in the nearby particle cloud as,

$$C(\mathbf{x},t) = \sum_{n=1}^{N} A_n f(\mathbf{x} - \mathbf{x_n}, R_n) \tag{30}$$

where A_n is the particle amplitude and is equal to particle volume, such that the integral of concentration field over space equals the sum of the volume of individual particles. Particle concentration around the nodal points in the Fluid model is computed based on the particle cloud radius with nodal point as centre.

To study the effect of non-Newtonian nature, we employ a power law. Here, μ is a function of the rate of deformation tensor $\mathbf{\Delta}$. For a two-dimensional problem, the shear strain rate computed as $\dot{\gamma} = \sqrt{\frac{1}{2}\mathbf{\Delta}_{II} : \mathbf{\Delta}_{II}}$. In the power law model used the viscosity is defined as,

$$\mu = K\dot{\gamma}^{n-1} \tag{31}$$

where, K (0.785) is the consistency index (Pas^n) and n (0.35) is the power law index [45]. For limiting the maximum non-Newtonian viscosity value, the minimum stain rate has been limited to $10^{-4}s^{-1}$. Also the typical Newtonian viscosity value of plasma, ($\mu_0 = 0.0012kgm/s$), has been used as the reference value for non-dimensionalising the viscosity of the blood.

4 Implementation of RBC aggregation

4.1 Initial RBC distribution

The problems studied require an initial distribution of RBCs to start the computation. In the present study, the elliptically shaped RBCs are distributed over the channel with almost equal spacing and randomly perturbed with maximum distance between them of $1.4\mu m$. The initial RBC velocity at the centre is fixed equal to the fluid velocity and then randomly perturbed with uniform probability density by using a maximum value of velocity equal to half of the maximum inlet velocity at the inlet. The initial orientation of the RBCs are also distributed randomly about z axis. Based on these initial conditions the values of initial Euler parameters have been obtained.

4.2 Time integration and collision

In the present work, two different schemes for the time integration of Equations 4 and 5, the central finite difference and second order Adams Bashforth method, have been tested. The latter scheme was observed to be faster than the central difference scheme. Since the time scales involved in the collision and adhesion process is much smaller than fluid time scale, the Adams Bashforth scheme is more suitable than the central difference scheme due to higher order of accuracy.

Due to different time scales of fluid flow, non-collided RBCs and collided RBCs, three different timescales are required to represent the system [21]. Thus three different time stepping procedures are introduced, one for solving the fluid dynamics equations, second for solving the transport of free RBCs and the last one for dealing with RBCs in contact. After a fluid time step, RBC velocities are calculated and collision is detected using particle convective timescale, which is one order less than the fluid time step. Following this, the collided RBCs are grouped together and a collision time step scale of the order $T_c = O[d(\rho_p^2/E_p^2U)^{(1/5)}]$, where E_p- particle effective elastic modulus, is used to solve the transport of aggregates [21].

While carrying out the computation, each RBC has the list of neighbouring particles within a preassigned radius and the number of particles in the local list contains approximately 45-60 RBCs. This allows an efficient search procedure to determine whether the particles are within the collision distance. Since RBCs form a rouleaux by lining up along the flat faces, the collision is assumed to have occurred when the distance between two RBCs is less than or equal to two semi-minor radius. Identification of contact points are important to find the normal and tangential components of adhesion forces between collided particles. This is computed using the quadratic equation of an ellipse. The position vector of an ellipses e^j satisfies the

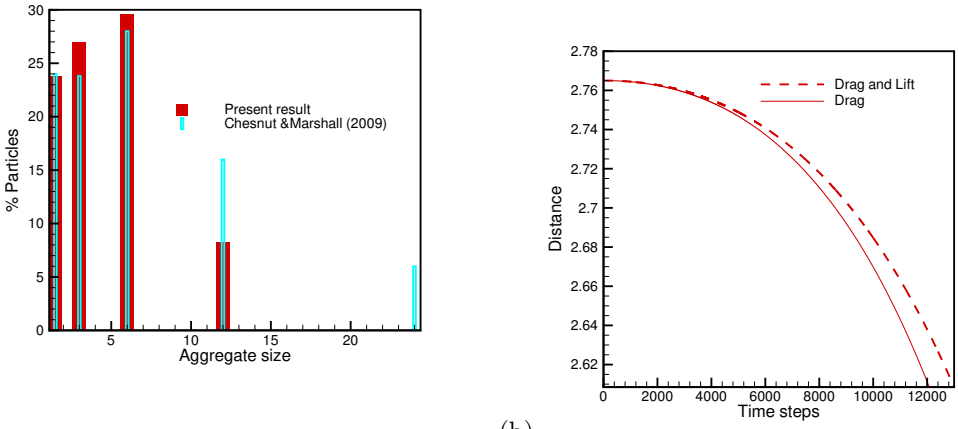

(a) (b)

Figure 2: (a) Percentage of particle aggregation at time=100sec, (b) Comparison of particle path with different hydrodynamic forces.

quadratic equation of an ellipse e^i at contact points. The surface of an ellipse can be represented by the quadratic equation in terms of canonical coordinates as,

$$XQ_iX^T = 0. \tag{32}$$

where $Q_i = \begin{bmatrix} 1/a^2 & 0 & 0 \\ 0 & 1/b^2 & 0 \\ 0 & 0 & -1 \end{bmatrix}$ is a characteristic matrix of an ellipse i and X is the position vector. If any vector $X = [x \quad y \quad 1]$ exists, such that the above equation is satisfied for two different ellipses, with characteristic matrix of Q^1 and Q^2, then the corresponding point (x, y) lies on both the ellipses.

5 Results and Discussions

The fluid dynamics model used here has been widely and thoroughly tested for both Newtonian and non-Newtonian blood flows in the past [31, 46, 30]. This flow model has been extended in the present study for the simulation of RBC aggregation and estimation of haemorheological changes in the microcirculation. However, benchmarking of RBC aggregation model is necessary and we use the data published[21] to qualitatively and quantitatively verify the results obtained using the present model.

5.1 RBC aggregation

It is of fundamental interest to check whether or not the results obtained are sensible and close to the results obtained by others. To do this, a microchannel of $700 \times 140\mu m$ is considered for the simulation of RBC aggregation in a two dimensional domain. The shear rate of $5.08s^{-1}$ is considered with no slip condition on the walls. While the lower wall is static, the upper wall is allowed to move at a prescribed velocity. After the flow simulation with Newtonian blood flow assumption, the RBCs are introduced into the plasma with a hematocrit value of 40 percent. The initial RBC distribution has resulted in an equilibrium surface energy value of 1.0×10^{-4} dyne/cm. Figure 2a shows the percentage of RBC aggregation at the time instant of 100 sec and as seen it is also compared with the published results. It is apparant that, the result shows an excellsent agreement with the existing result of [21] for smaller aggregation sizes. The disagreement for larger aggregates may be the result of differences in initial conditions employed and the addition of lift forces to the model.

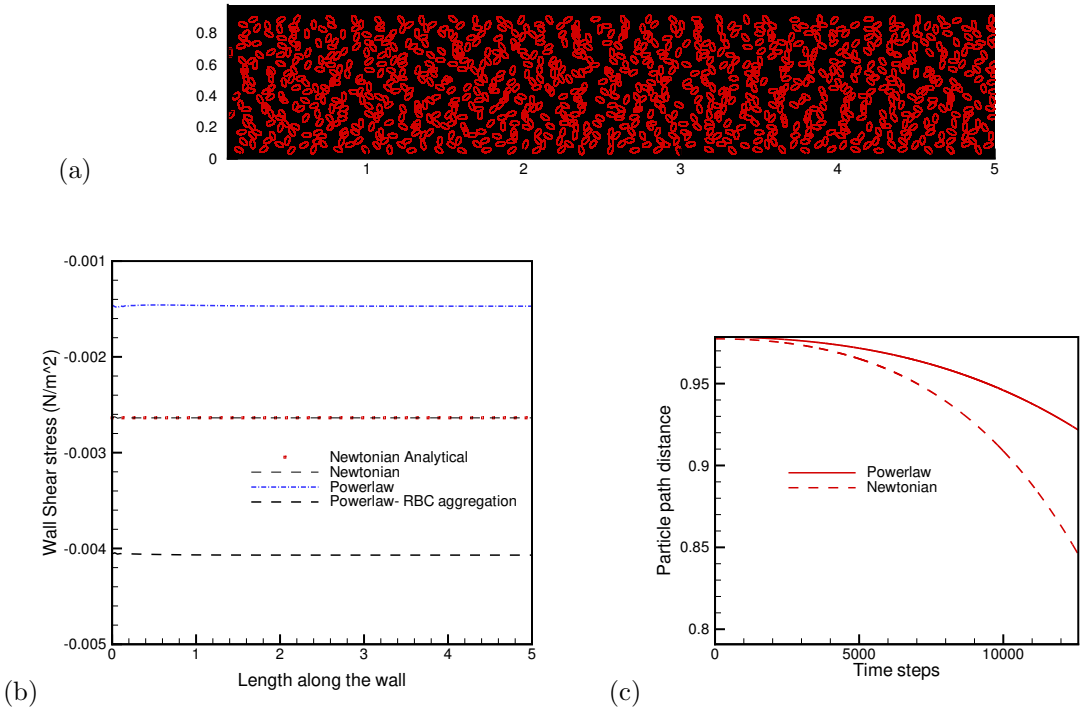

Figure 3: (a) RBC aggregation in the channel flow at $t = 100sec$, (b) Comparison of wall shear stress variation along the wall-dimensional $H = 40, Re = 20$, (c) Comparison of particle path between Newtonian and Powerlaw flow with RBC aggregation

5.2 Impact of lift force

Since the lift force of the particles have been ignored in the past, it is of interest to understand the impact of the lift force. To demonstrate the impact of the lift force, the time trajectory of an RBC at $385 \times 105\mu m$ is computed and plotted with and without lift force as shown in Figure 2b. As seen the RBC with the lift and drag forces takes a slightly longer path than the RBC with only drag force. Although the difference is small, the wider impact of this lift force in complex arteries may be significant. Thus, neglecting the lift force may lead to erroneous computation of RBC aggregation.

5.3 Impact of RBC aggregation on rheological changes

The haemorheological changes of blood flow in the channel have been investigated here using the powerlaw model explained in the previous section. A channel of $700 \times 140\mu m$ has been considered again with no slip conditions on both the lower and upper walls. A fully developed flow condition at the inlet is used for the simulation of flow field. Figure 3a shows the RBC aggregation at the time instant of 100 sec for a shear rate of $5.08s^{-1}$. It is evident from this figure that the bigger aggregates are formed at the centre of the channel. It is also observed that aggregated RBCs have the tendency to move away from the walls. This is due to the fact of shear rate is lower at the centre of the channel and higher closer to the walls. The results observed is inline with the experimental results reported in the literature [47, 2]. This phenomenon is responsible for the formation of a cell-free layer closer to the wall. This phenomenon is normally prominent in tubes of diameters smaller than $400\mu m$ [3]. Formation of cell free layer reduces the RBC concentrations near the vessel walls and responsible for lower viscosity here.

Figure 3b shows the wall shear stress for different flow conditions at the time instant of 100sec. Compar-

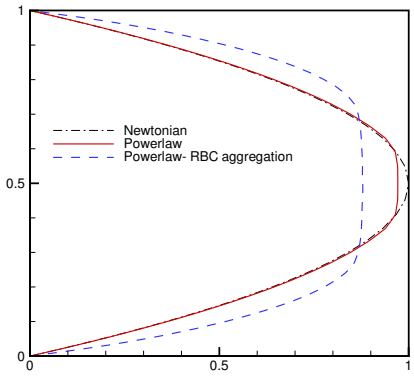

Figure 4: Velocity profile comparison between Newtonian, powerlaw and powerlaw with RBC aggregation across a section for $H = 40, Re = 20$

ison of wall shear stress value for Newtonian flow assumption bewtween numerical ($-2.63\times10^{-3}N/m^2$) and analytical ($-2.63\times10^{-3}N/m^2$) solution shows excellent agreement. The results also show a considerable difference in wall shear stress between Newtonian and Powerlaw fluid. As seen wall shear stress value is higher when the powerlaw is introduced. However when the powerlaw is combined with aggregation, a dramatic drop in the value of wall shear stress is noticed. This result clearly demonstrates why powerlaw models can not be used in isolation without RBC aggregation.

Figure 3c shows the particle path over time for Newtonian and Powerlaw model with RBC aggregation. The result shows considerable difference and it is observed that the Powerlaw fluid show longer path due to shear thinning behaviour. As observed in the sensitivity study with drag and lift forces on particle path, Powerlaw fluid takes a longer path than Newtonian flow. Once again it is ascertained that due to RBC aggregation and shear thinning property of flow, fluid forces are very different.

Velocity profiles at different sections of the channel have been plotted and compared with the velocity computed under Newtonian flow assumption and are shown in Figure 4. The velocity profile shows tremendous difference, which necessitates the need for studying haemodynamics under shear thinning flow assumption. Velocity profile at the centre of the channel shows highly blunted shape due to the RBC aggregation and clustering, similar flow behaviour has been reported by [2] in microvessel under *in-vivo* study. Velocity profile based on *in-vivo* study for slow flow with aggregation has been proposed in the past and given an exponent value for K=3.8 [25] for the velocity profile as,

$$V(r) = V_{max}\left(1.0 - \left|\frac{r}{R}\right|^K\right) \tag{33}$$

In the present study, predicted velocity profile gives a value of K=3.7.

Figures 5 to 6 show the velocity and viscosity variation across the channel for different shear rates. It is clearly evident from the figures that the aggregation increases the viscosity at the centre of the channel. Figures 5a and 5b show the velocity variation and viscosity contours predicted with RBC aggregation for $Re = 20$ at heatocrit of 40%. As expected the viscosity is increased due to bigger aggregation at the centre of the channel. Viscosity of flow is lower in the near wall region due to reduced RBC concentration and increased shear rate. This increased shear rate causes the breaking up of rouleau and reduction in particle concentration as indicated in [48]. From the figures it is clear that viscosity variation due to RBC aggregation has a major impact on velocity distribution across the channel. At higher Reynolds numbers ($Re = 50$), the viscosity (Fig. 6b) is lower, which is anticipated at higher shear rates. Figure 7a shows the RBC aggregation for the hematocrit value of 30% and $Re = 20$. From the figure 7b it is observed that viscosity values have been decreased compared to the viscosity values at 40% hematocrit. This is a result of reduction in number of RBCs.

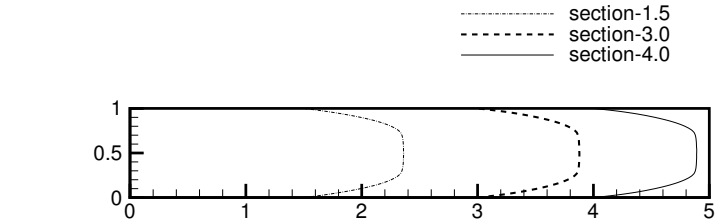

(a)

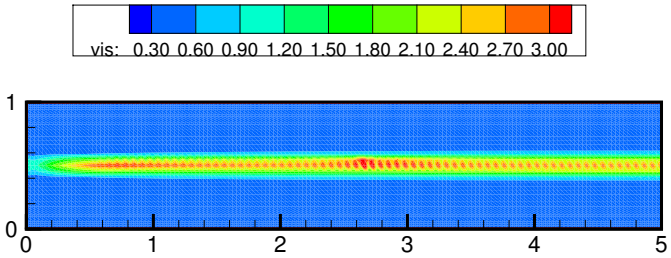

(b)

Figure 5: (a) Velocity profile at different sections, (b) Viscosity contours, for $H = 40, Re = 20$

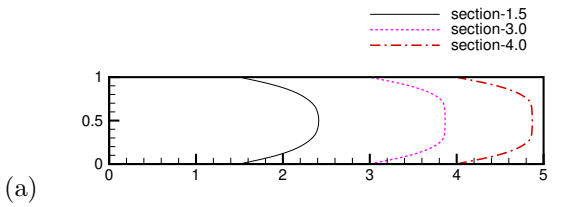

(a)

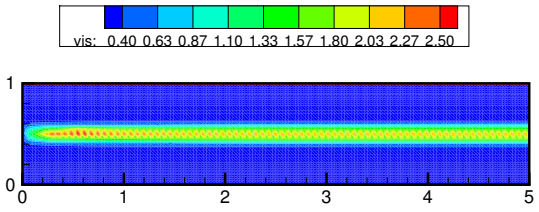

(b)

Figure 6: (a) Velocity profile at different sections (b) Viscosity contours (c) Wall shear stress, for H=40, Re=50

(a)

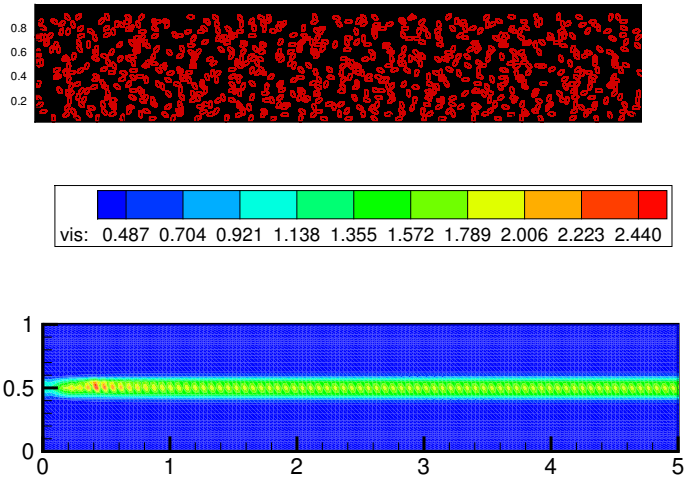

(b)

Figure 7: (a) RBC Aggregation (b) Viscosity contours (c) Wall shear stress for H=30, Re=20

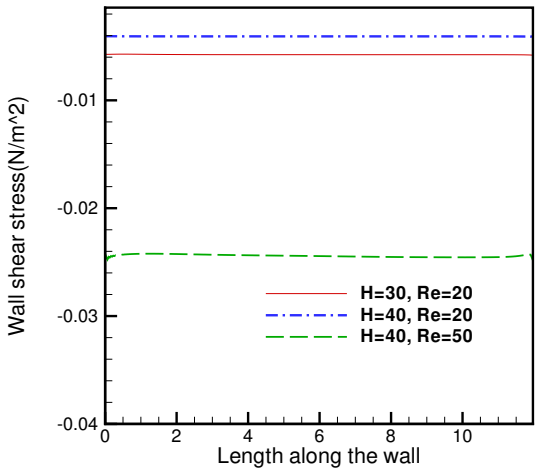

Figure 8: Comparison of shear stress

Wall shear stress along the length of the channel has been compared for different hematocrit values and Reynolds numbers in Figure 8. The figure clearly shows that increase in shear rate dramatically reduces the viscosity values and thus wall shear stress. The figure also shows that increase in RBC concentration increases the viscosity and thus the wall shear stress.

6 Concluding summary

A numerical model has been developed for simulating RBC aggregation in the microchannel based on receptor-ligand binding model and tested with published results. The model is capable of predicting RBC aggregation and the effect of aggregation on rheological characteristics of blood flow in the microchannel flow. From the investigations, it is observed that the results show clear evidence of increase in the viscosity due to rouleau formation and resulted in reduction of wall shear stress. A sensitivity study shows the shear induced lift has significant effect on particle path and RBC aggregation. In the computational model Powerlaw model has been incorporated to study the non-Newtonian flow characteristics. Hematocrit value of particles has been varied to study the aggregation effect on viscosity and it is observed that for higher haematocrit value the viscosity also increased under RBC aggregation.

7 Acknowledgement

This work was fully supported by Royal Society, London under Newton Fellowship, reference NF100532.

References

[1] Mchedlishvili G., L. Gobejishvili, and N.Beritashvili. Effect of intensified red blood cell aggregability on arterial pressure and mesenteric microcirculation. *Microvasc.Res.*, 45:233, 1993.

[2] Bishop J.J., P.R. Nance, A.S. Popel, M.Intaglietta, and P.C. Johnson. Effect of erythrocyte aggregation on velocity profiles in venules. *Am. J.Physiol*, 280:H222–H236, 2001.

[3] Kim S., A.S. Popel, M. Intaglietta, and P.C. Johnson. Effect of erythrocyte aggregation at normal human levels on functional capillary density in rat spinotrapezius muscle. *Am. Jl. of Phys. Heart and Circ. Phys.*, 290, 2006.

[4] Chien S. Biophysical behaviour of red cells in suspensions. *In: The red blood cell. D.M. Surgenor , Ed., Academic Press, New York*, pages 1031–1133, 1975.

[5] Lowe G.D.O. and Barbenel J.C. Plasma and blood viscosity. *In: Clinical blood rheology. G.D.O. Lowe, Ed., CRC Press Inc.,Florida*, pages 1–10, 1988.

[6] Perkkio J., L.J. Wurzinger, and H. Schmid-Schonbein. Plasma and platelet skimming at t-junctions. *Thrombosis Res.*, 45:517–526, 1987.

[7] Pries A.R., K. Ley, M. Claassen, and P.Gaehtgens. Red cell distribution at microvascular bifurcations. *Microvasc. Res.*, 38:81–101, 1989.

[8] Lipowsky HH., Cram LE., Justice W., and Eppihimer MJ. Effect of erythrocyte deformability on in vivo red cell transit time and hematocrit and their correlation with in vitro filterability. *Microvasc Res.*, 46:43–64, 1993.

[9] Dintenfas L. Blood micro-rheology viscosity factorsin blood flow, ischemia and thrombosis (1971 butterworth press), rheology of blood in diagnostic and preventive medicine, (1976 butterworth press), hyperactivity and hypertension and blood viscosity in heart disease and cancer (1981 pergamon press) plus numerous medical papers. 1971.

[10] Demiroglu H.and I Barista and S. Dndar. Erythrocyte aggregability in patients with coronary heart disease. *Clinical Hemorheology*, 16, 1996.

[11] Fleming I., Bauersachs J., and Busse R. Calcium-dependent and calcium-independent activation of the endothelial no synthase. *Jl. Vasc.Res.*, 34:165–174, 1997.

[12] Chein S., S. Usami, and Jhon F. Bertles. Abnormal rheology of oxygenated blood in sickle cell anemia. *The Jl. Clin. Investn.*, 49:623–634, 1970.

[13] Rainer R., D.T. Kawanishi, P. Anthony, N. Chandraratna, R.M. Bauersachs, C.L. Reid, S.H. Rahimtoola, and H.J. Meiselman. Changes in blood rheology in patients with stable angina pectoris as a result of coronary artery disease. *Circulation*, 76(1):15–20, 1987.

[14] Pozrikidis C. Finite deformation of liquid capsules enclosed by elastic membranes in simple shear flow. *Jl. of Fluid Mechanics*, 297:123–152, 1995.

[15] Agresar G., Linderman JJ., Tryggvason G., and Powell KG. An adaptive, cartesian, front-tracking method for the motion, deformation and adhesion of circulating cells. *J. Comput Phys.*, 143:346–380, 1998.

[16] Liu Y., Zhang L., Wang X., and Liu WK. Coupling of navier-stokes equations with protein molecular dynamics and its application to hemodynamics. *Int. Jl. of Num. Methods in Fluids*, 46:1237–1252, 2004.

[17] NDri NA., Shyy W., and Tran-Son-Tay R. Computational modeling of cell adhesion and movement using a continuum-kinetics approach. *Biophys Jl.*, 85:2273–86, 2003.

[18] Bagchi P., Johnson PC., and Popel AS. Computational fluid dynamic simulation of aggregation of deformable cells in a shear flow. *J. Biomech Eng.*, 127:1070–1080, 2005.

[19] Bell GI., Dembo M., and Bongrand P. Cell adhesion, competition between nonspecific repulsion and specific bonding. *Biophys. Jl.*, 45:10511064, 1984.

[20] Hammer D.A and Sachin M. Apte. Simulation of cell rolling and adhesion on surfaces in shear flow: general results and analysis of selectin-mediated neutrophil adhesion. *Biophys. Jl.*, 63:35–57, 1992.

[21] Chesnutt J.K.W and J.S. Marshall. Blood cell transport and aggregation using discrete ellipsoidal particles. *Comp. Fluids*, 38:1782–1794, 2009.

[22] Chesnut and Marshall. Effect of particle collisions and aggregation on red blood cell passage through a bifurcation. *Microvascular Res.*, 78:301–313, 2009.

[23] Marshall J.S. Particle dispersion in a turbulent vortex core. *Physics of Fluids*, 17(2):025104–1–025104–15, 2005.

[24] Goldsmith H. L., D. N. Bell, S. Spain, and F.A. McIntosh. Effect of red blood cells and their aggregates on platelets and white cells in flowing blood. *Biorheology*, 36:461468, 1999.

[25] Bishop J.J., A.S. Popel, M. Intaglietta, and P.C. Johnson. Effects of erythrocyte aggregation and venous network geometry on red cell axial migration. *Am. J. Physiol.*, 281(2):H939–950, 2001.

[26] Bagchi P. Mesoscale simulation of blood flow in small vessels. *Biophysical Jl.*, 92:18581877, 2007.

[27] Murata T. Effects of sedimentation of small red blood cell aggregates on blood flow in narrow horizontal tubes. *Biorheology*, 33:267–283, 1996.

[28] Das B., G. Enden, and A. S. Popel. Stratified multiphase model for blood flow in a venular bifurcation. *Ann. Biomed. Eng.*, 25:135153, 1997.

[29] Johnston B.M., Johnston P.R., Corney S., and Kilpatrick D. Non-newtonian blood flow in human right coronary arteriea: steady state simulations. *Jl. of Biomechanics*, 37:709–720, 2004.

[30] Chitra K., T. Sundararajan, S. Vengadesan, and P. Nithiarasu. Non-newtonian blood flow study in a model cavopulmonary vascular system. *Int. J. Num. Meth. Fluids*, 66:269–283, 2011.

[31] Nithiarasu P. An efficient artificial compressibility (ac) scheme based on the characteristic based split (cbs)method for incompressible flows. *Int. Jl. for Num. Meth. Engg.*, 56:1815–1845, 2003.

[32] Zienkiewicz O.C., R.L. Taylor, and P. Nithiarasu. The finite element method for fluid dynamics, sixth edition. *Elsevier*, 2005.

[33] Goldstein H. Classical mechanics. *2nd Ed. Addison-Wesley, Reading, MA.*, 1980.

[34] Brenner H. The stokes resistance of an arbitrary particle-iv, arbitrary fields of flow. *Chem. Eng.Sci.*, 19:703–727, 1964.

[35] Di Felice R. The voidage function for fluidparticle interaction systems. *Int J Multiphase Flow*, 20:1539, 1994.

[36] Fan F.G. and Ahmadi G. A sublayer model for wall deposition of ellipsoidal particles in turbulent streams. *J.Areosol. Sci.*, 26:813–840, 1995.

[37] Harper E.Y. and Chang I.D. Maximum dissipation resulting from lift in a slow viscous shear flow. *J. Fluid Mech.*, 33:209–225, 1968.

[38] Chokshi A., Tielens AGGM., and Hollenbach D. Dust coagulation. *Astrophysics Jl.*, 407:806–819, 1993.

[39] Katchalsky A., 0. Kwnsm, C. KLIBANSKY, and A. DEVum. In flow properties of blood and other biological systems. *A. L. Copley and G. Stainsby, editors. Pergamon Press, New York.*, 155:166, 1960.

[40] Mindlin R.D. Compliance of elastic bodies in contact. *Jl. of Applied Mechanics*, 16:259268, 1949.

[41] Tsuji Y., T. Tanaka, and T. Ishida. Lagrangian numerical simulation of plug flow of cohesionless particles in a horizontal pipe. *Powder Technology*, 71:239250, 1992.

[42] Dominik c. and A.G.G.M. Tielens. Resistance to rolling in the adhesive contact of two elastic spheres. *Philosophical Magazine A*, 92(3):783803, 1995.

[43] Kuhn M.R. and K. Bagi. Alternative definition of particle rolling in a granular assembly. *J. Eng. Mech.*, 130:826835, 2004.

[44] Marshall J.S. Discrete-element modeling of particle aerosol flows. *Jl. of Computational Physics*, 228:1541–1561, 2009.

[45] Neofytou P. Transition to asymmetry of generalized newtonian fluid flows through a symmetric sudden expansion. *J. Non-Newtonian Fluid Mechanics*, 133:132–140, 2006.

[46] Chitra K., S.Vengadesan, T.Sundararajan, and P. Nithiarasu. An investigation of pulsatile flow in a model cavo-pulmonary vascular system. *Comm. in Num. Meth. in Engg.*, 25:1061–1083, 2008.

[47] Reinke W., Gaehtgens P., and Johnson PC. Blood viscosity in small tubes: effect of shear rate, aggregation and sedimentation. *Am. Jl. Physiol.*, 253:540547, 1987.

[48] Riha S.P. Time-dependent formation of red blood cell aggregates and its influence on blood rheological behaviour. *Biological Physics*, 19(1):65–70, 1993.